

Corrected: Author Correction

Electronic correlations in twisted bilayer graphene near the magic angle

Youngjoon Choi^{1,2,3}, Jeannette Kemmer^{1,2}, Yang Peng^{2,3,4}, Alex Thomson^{2,3,4}, Harpreet Arora^{1,2}, Robert Polski^{1,2}, Yiran Zhang^{1,2,3}, Hechen Ren^{1,2}, Jason Alicea^{2,3,4}, Gil Refael^{2,3,4}, Felix von Oppen^{2,5}, Kenji Watanabe^{1,2}, Takashi Taniguchi⁶ and Stevan Nadj-Perge^{1,2,4}

Twisted bilayer graphene with a twist angle of around 1.1° features a pair of isolated flat electronic bands and forms a platform for investigating strongly correlated electrons. Here, we use scanning tunnelling microscopy to probe the local properties of highly tunable twisted bilayer graphene devices and show that the flat bands deform when aligned with the Fermi level. When the bands are half-filled, we observe the development of gaps originating from correlated insulating states. Near charge neutrality, we find a previously unidentified correlated regime featuring an enhanced splitting of the flat bands. We describe this within a microscopic model that predicts a strong tendency towards nematic ordering. Our results provide insights into symmetry-breaking correlation effects and highlight the importance of electronic interactions for all filling fractions in twisted bilayer graphene.

he electronic properties of metals, insulators and semiconductors are frequently described in the framework of non-interacting electrons. This description works remarkably well when the kinetic energy of electrons at the Fermi energy, as set by the dispersion of the electronic bands, is large compared with the Coulomb interaction. However, the kinetic energy is quenched in materials with almost non-dispersive—or flat—bands. In these materials, interactions between electrons may generate strongly correlated electronic phases. Twisted bilayer graphene (TBG) has recently emerged as a highly tunable and surprisingly simple platform for the experimental investigation of such strongly correlated phases^{1–3}. Two layers of graphene are stacked with a twist angle of θ and form a periodic moiré pattern (Fig. 1a), localizing electronic wave functions^{4–7} in regions in which carbon atoms are stacked on top of each other (AA stacking).

While monolayer graphene is accurately described in terms of free Dirac electrons⁸, in a bilayer, hybridization significantly alters the electronic band structure, particularly when the layers are twisted by a small angle θ <3° (refs. $^{9-17}$). In this case, interlayer hybridization yields two low-energy bands separated by a gap from the higher-energy dispersive bands (Fig. 1b,c)^{5-7,18-20}. The resulting Van Hove singularities (VHS) generate maxima in the local density of states and can be probed directly using scanning tunnelling microscopy (STM)^{10,11,21,22}. As the twist angle is reduced, the VHS move closer together. Finally, close to the magic angle value $\theta \approx 1.1^{\circ}$ (ref. 5) the bands become highly non-dispersive.

Near the magic angle, electron–electron interactions modify the electronic properties of TBG due to the quenching of the kinetic energy. Interaction effects have been observed in recent transport experiments^{1–3,17}, which reveal the existence of correlated insulating and superconducting states. The strong correlations along with a large number of atoms in a moiré unit cell pose substantial challenges to a microscopic understanding of this system. Local probes

such as STM can therefore provide invaluable information, both on the electronic band structure and correlation effects.

Figure 1d outlines the experimental set-up. The starting point is a van der Waals structure consisting of twisted bilayer graphene placed on top of a thin boron nitride (BN) layer. A metallic graphite multilayer of approximately 10 nm thickness resides underneath the BN and serves as a back gate. The twisted bilayer and the back gate are contacted separately using predefined gold electrodes. Our setup differs from previous STM measurements¹⁴⁻¹⁶ on gated bilayer graphene by the careful alignment of the graphene layers close to the magic angle and the use of a graphite back gate to reduce disorder effects^{3,23}. Unlike in the samples used for transport studies, the TBG in our experiments is not covered by BN (Fig. 1e; see also Supplementary Section 1). In line with the previous experiments3,14,24, we find that our TBG is not uniform across the entire sample, forming domains with different local twist angles. We show results from two devices with domains exhibiting angles in the range $1^{\circ} < \theta < 2^{\circ}$ measured at an effective temperature of $T = 1.5 \,\mathrm{K}$ as calibrated on the superconducting gap of a lead crystal.

Figure 1f,g shows topographies of two devices with distinct moiré superlattice periodicities of $L_{\rm M}\!\approx\!7\,{\rm nm}$ (Fig. 1f, device D1) and $L_{\rm M}\!\approx\!13\,{\rm nm}$ (Fig. 1g, device D2). We estimate a local twist angle θ from the area of the moiré unit cell and find $\theta\!=\!1.92^{\circ}$ and $\theta\!=\!1.01^{\circ}$, respectively. The topographies show an apparent periodic height increase of approximately 3–8 Å that reflects the increased local density of states of the AA stacking regions, confirming the formation of a moiré lattice⁶. We typically observe that the moiré superlattice is not strictly three-fold symmetric as the periods in the three directions can differ by approximately 5–10%.

Figure 1h,i shows the observed point spectra for the non-magic twist angle θ =1.92° at various back-gate voltages V_{Bg} . All point spectra are taken on AA regions where the flat bands predominately localize. The two peaks in the local tunnelling density of states

¹T. J. Watson Laboratory of Applied Physics, California Institute of Technology, Pasadena, CA, USA. ²Institute for Quantum Information and Matter, California Institute of Technology, Pasadena, CA, USA. ⁴Walter Burke Institute for Theoretical Physics, California Institute of Technology, Pasadena, CA, USA. ⁵Dahlem Center for Complex Quantum Systems and Fachbereich Physik, Freie Universität Berlin, Berlin, Germany. ⁶National Institute for Materials Science, Tsukuba, Ibaraki, Japan. *e-mail: s.nadj-perge@caltech.edu

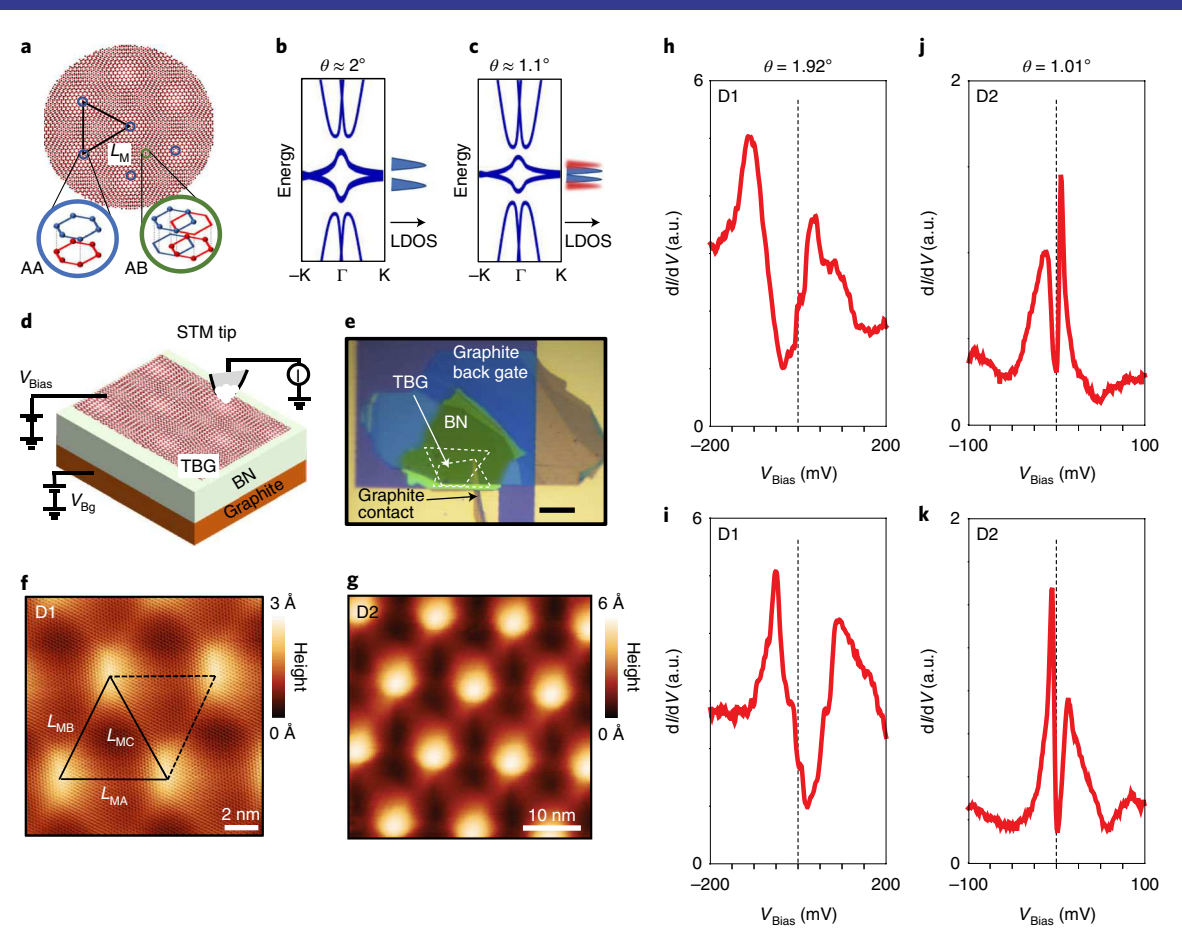


Fig. 1 | Twisted bilayer graphene. a, The twist angle θ in TBG gives rise to the formation of a triangular moiré lattice of regions corresponding to AA stacking (blue circles and corresponding inset) with the period $L_{\rm M}$ separated by AB and BA stacking regions (green circle and corresponding inset). A large DOS is expected to be localized on the AA regions^{4–6}. **b,c**, Schematics of the TBG band structure and the corresponding DOS showing VHS peaks. For angles close to θ =1.1°, correlations are expected to deform the VHS peaks (marked in red). **d**, Experimental set-up. TBG is placed on top of an atomically smooth dielectric (BN) and back gated by an approximately 10-nm-thick graphite layer. **e**, Optical image of the sample. Dashed areas correspond to two graphene layers. Scale bar, 20 μm. **f**, Topography showing the moiré pattern for the θ =1.92° area of device D1. Note that $L_{\rm M}$ is not identical for the different directions ($L_{\rm MA}$ =7.1 nm, $L_{\rm MB}$ =7.6 nm, $L_{\rm MC}$ =7.3 nm), indicating small external strain in the sample. Set-point conditions: set-point voltage $V_{\rm s}$ =-200 mV and set-point current $I_{\rm s}$ =50 pA. **g**, Topography for the θ =1.01° area of device D2 ($L_{\rm MA}$ =13.8 nm, $L_{\rm MB}$ =13.7 nm, $L_{\rm MC}$ =14.2 nm). Set-point conditions: $V_{\rm s}$ =500 mV and $I_{\rm s}$ =50 pA. **h,i**, Spectroscopy on an AA site (device D1) for the slight electron (**j**, $V_{\rm Bg}$ =-0.6 V) and hole (**k**, $V_{\rm Bg}$ =-3.6 V) doping for θ =1.01°. a.u., arbitrary units.

(TDOS) are identified as VHS separated by approximately 150 meV. This splitting is consistent with previous STM results for similar angles 10 . Changing the position of the Fermi level relative to the VHS via the back gate shifts the positions of the two peaks in bias voltage but leaves their separation and overall line shape approximately unchanged. This is consistent with a simple band-structure picture (see Supplementary Section 2 for data at larger θ).

For regions near the magic angle (θ =1.01°), the observed spectra differ qualitatively (Fig. 1j,k). Here, the overall shapes of the peaks change as they approach the Fermi energy ($V_{\rm Bias}$ =0 mV). The peak approaching the Fermi level sharpens and increases in height, signalling a rapid decrease in lifetime broadening. This feature is seen for both electron and hole doping. Moreover, the splitting between the peaks is highly sensitive to $V_{\rm Bg}$, indicating that electronic correlations cause deviations from a simple band-structure picture of the flat bands.

Figure 2a illustrates the detailed evolution of the local TDOS as a function of electron density for device D1 (θ =1.04°, $L_{\rm MA}$ =14.3 nm; $L_{\rm MB}$ =13.3 nm; $L_{\rm MC}$ =13.3 nm, as defined in Fig. 1f). We show here data from D1 since higher doping levels could be accessed in this

device due to a slightly thinner gate dielectric. When the electronic flat bands sit below the Fermi level (3.8 V < V_{Bg} < 10 V, green region in Fig. 2a), the completely filled bands shift linearly as V_{Bg} is reduced. The slope of $\Delta V_{\rm Be}/\Delta V_{\rm Bias} \approx 1 \, {\rm V}/5 \, {\rm mV}$ is directly proportional to the density of states (DOS) $\Delta n/\Delta \mu$ at the Fermi level in the regimes where electronic correlations are weak (with n being the carrier concentration and μ the chemical potential). When the DOS is high, the slope $\Delta V_{\mathrm{Bg}}/\Delta V_{\mathrm{Bias}}$ is large as substantial changes in the back-gate voltage are needed to shift the chemical potential. In the opposite limit, when the Fermi level passes through a gapped region, the slope $\Delta V_{\rm Bg}/\Delta V_{\rm Bias}$ is close to zero. The linear shift of the peaks for $3.8\,{\rm V}<{\rm V}_{\rm Bg}<10\,{\rm V}$ indicates a constant DOS as expected when the Fermi level is located in the non-flat bands (Fig. 2a,b, green regions). We note that even when bands are fully filled, the observed asymmetry of the TDOS peaks, reflected in the peak height, is more pronounced compared with areas with larger twist angle θ , possibly reflecting the absence of electron-hole symmetry in the system²⁵⁻²⁷.

The slope is reduced in the gate range $2.7 \text{ V} < V_{\text{Bg}} < 3.8 \text{ V}$ (Fig. 2a,b, orange regions) just before the flat bands start to cross the

ARTICLES NATURE PHYSICS

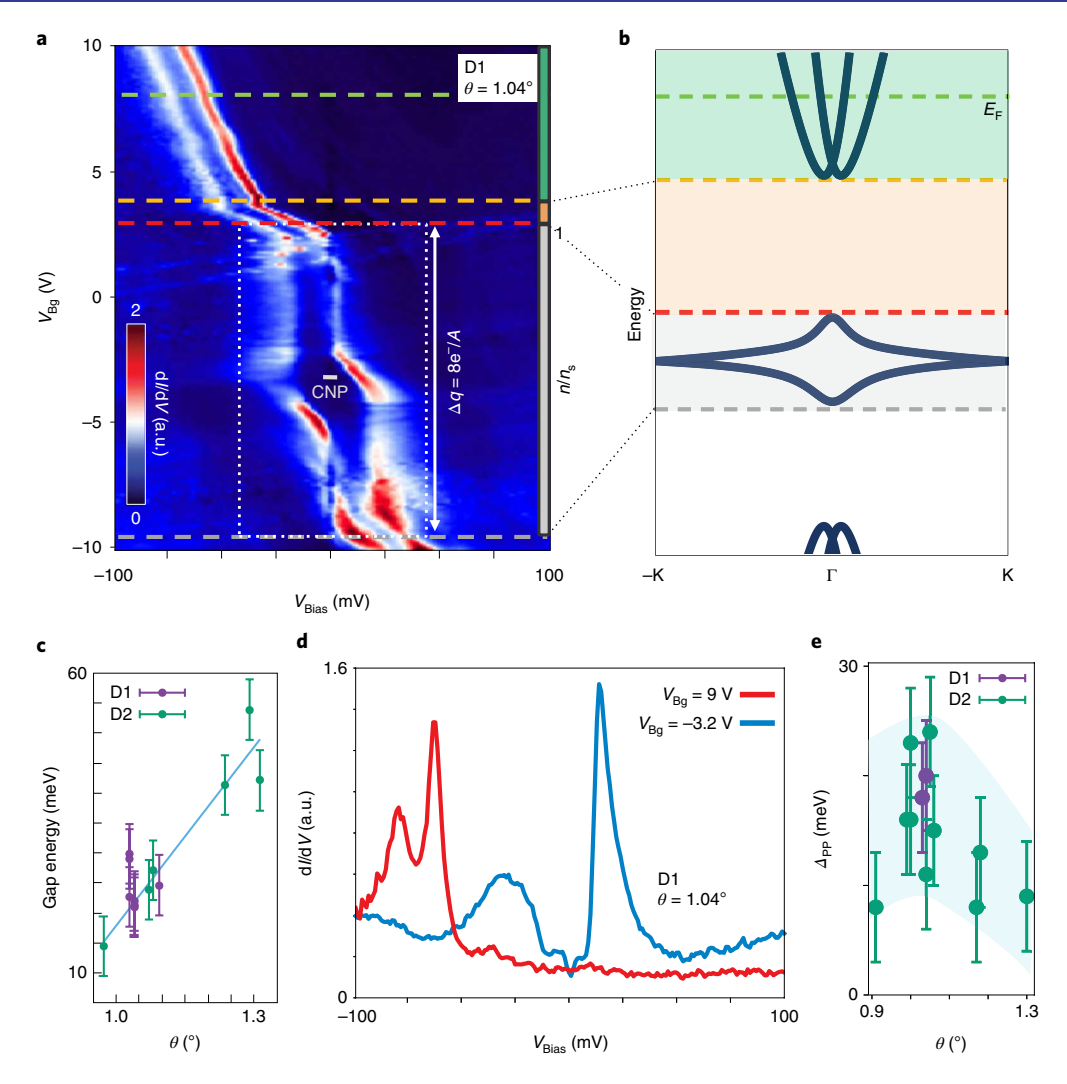


Fig. 2 | **Evolution of the TBG point spectrum with back-gate voltage. a**, Point spectra on an AA site as a function of $V_{\rm Bgr}$ which tunes the overall charge density and therefore the Fermi level. Coloured regions in the right side bar correspond to different regimes: green, Fermi level ($E_{\rm F}$) in the dispersive bands; orange, Fermi level in the gap; grey, Fermi level in the flat bands. The grey region indicates partial filling of the flat bands in units $n/n_{\rm s}$, where $n_{\rm s}$ is the charge density corresponding to four electrons per moiré unit cell. The white dashed rectangle highlights the flat bands, see also Fig. 3a. **b**, Schematic of the TBG band structure with colours indicating the different regimes shown in **a**: dispersive bands (green), bandgap (orange) and flat bands (grey). **c**, Gap between the electron flat band and the upper dispersive bands versus angle as extracted from similar conductance-map data obtained at different angles θ. The blue line is a guide to the eye. **d**, Line traces from **a** for fully occupied bands (red, $V_{\rm Bg}$ = 9 V) and close to the CNP (blue, $V_{\rm Bg}$ = -3.2 V). **e**, Difference between the peak separation at the CNP and at full-filling $\Delta_{\rm PP}$ as a function of angle θ evaluated by correcting for tip gating effects; see Supplementary Section 4 for details. We observe that the spatial tip offsets of the order of 1nm from the centre of the AA regions can cause a few mV shifts of the TDOS peak positions. The maximum value of this shift sets the error bars in **c** and **e** to be ±5 mV. The shaded region in **e** is a guide to the eye.

Fermi level. This observation indicates a gap between the flat and the upper dispersive band, of approximately 25 meV according to the total shift in the chemical potential over this range of $V_{\rm Bg}$. The finite slope in this region signals a remnant density of sub-gap states that likely originates from localized states often observed in STM measurements^{9,10,16}. We also find that the gap decreases for smaller twist angles (Fig. 2c) as predicted theoretically²⁸. The extracted gap values strongly suggest that the additional bands become increasingly important as the angle θ drops below 1° (ref. ⁵), thus setting a lower bound on the twist angle for observing correlated insulating states.

For $-9.5\,\mathrm{V} < V_{\mathrm{Bg}} < 3\,\mathrm{V}$ (Fig. 2a,b grey regions), the bands become distorted due to electronic correlations. We observe several suppressions of the TDOS at the Fermi level, and the slope $\Delta V_{\mathrm{Bg}}/\Delta V_{\mathrm{Bias}}$ changes repeatedly. First, the slope is large as the upper flat band, with its large DOS, crosses the Fermi level $(-1\mathrm{V} < V_{\mathrm{Bg}} < 2.7\,\mathrm{V})$.

In this region, suppressions of the TDOS near $V_{\text{Bias}} = 0 \,\text{mV}$ are observed (see Supplementary Section 6 for more data). As the upper flat band is depopulated, the slope $\Delta V_{\text{Be}}/\Delta V_{\text{Bias}}$ of the upper VHS peak decreases, while the slope of the lower peak barely changes, enhancing the apparent splitting between the bands. At $V_{\text{Bg}} \approx -3.2 \text{ V}$, the charge neutrality point (CNP) is reached. As V_{Bg} is reduced further, the splitting between the TDOS peaks is gradually reduced and then the peak corresponding to the lower flat band passes through the Fermi level. The total range of $\Delta V_{\rm Bg} \approx 13 \pm 1\,{\rm V}$ (grey region in Fig. 2a) over which the two flat bands cross the Fermi level is expected to change the charge density by $\Delta q = 8e^{-}/A = 1.6 \times 10^{-19}$ $C \times 5.46 \times 10^{12}$ cm⁻² (A is the measured area of this moiré unit cell), corresponding to filling of the two bands by a total of 8 electrons per moiré unit cell. This matches the change in charge density extracted experimentally based on the gate capacitance for a BN thickness $d_{\rm BN}$ = 40 nm, as measured by atomic force microscopy (AFM), and

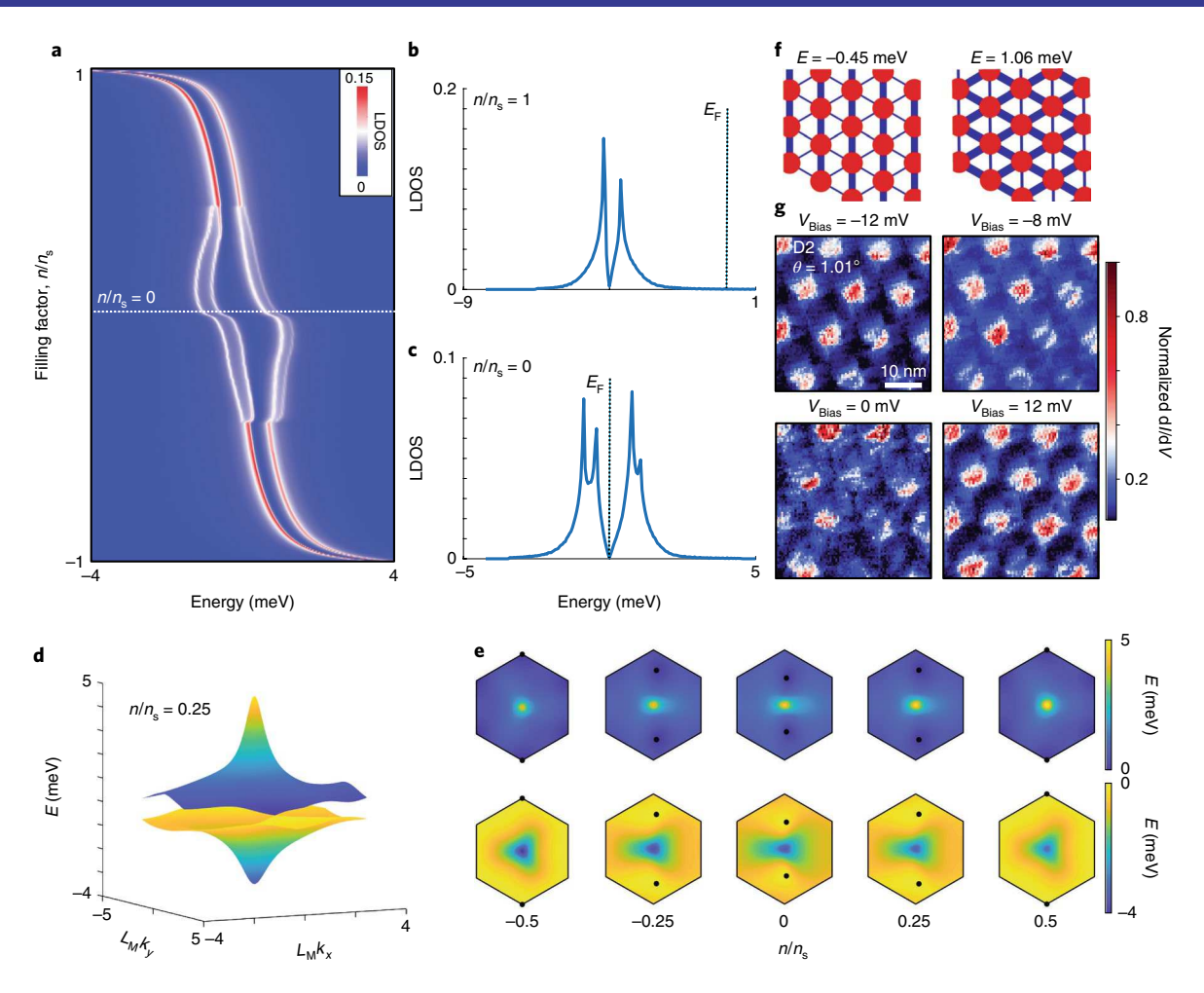


Fig. 3 | **Model calculations and breaking of** C_3 **symmetry. a**, DOS as a function of energy and filling factor n/n_s for a single-flavour ten-band model with short-range Coulomb interactions. The value of $E_c/W=1$ is chosen to qualitatively match the experiment upon an overall scaling factor. **b,c**, Line cuts at filling factor $n/n_s=1$ (**b**) and $n/n_s=0$ (**c**), which demonstrate the enhanced splitting at the CNP and broadening of the peaks compared with the non-interacting model. **d**, Calculated band structure across the Brillouin zone showing the position of the Dirac points at the CNP for a C_3 -broken state at $n/n_s=0.25$. **e**, Band structure obtained from the C_3 -broken state for different filling factors (left to right $n/n_s=-0.5$, -0.25, 0, 0.25, 0.5). Upper (lower) panels correspond to the electron (hole) band; black dots indicate locations of the Dirac points. **f**, Calculated LDOS profiles at the domain walls connecting different AA sites, represented with lines of width directly proportional to the LDOS (see Supplementary Section 7 for more details). **g**, Spatially resolved TDOS maps near the CNP highlighting anisotropy at different bias voltages V_{Bias} (with $V_{\text{Bg}} = -4.5 \,\text{V}$). From the upper left corner to the lower right: $-12 \,\text{mV}$, $-8 \,\text{mV}$ (upper panels); 0 mV, 12 mV (lower panels). Data were taken at the $\theta = 1.01^\circ$ area of device D2 ($L_{\text{MA}} = 13.8 \,\text{nm}$, $L_{\text{MB}} = 13.7 \,\text{nm}$, $L_{\text{MC}} = 14.2 \,\text{nm}$) with the open feedback and set-point conditions $V_s = 500 \,\text{mV}$ and $I_s = 200 \,\text{pA}$.

dielectric constant $\varepsilon_{\rm BN} \approx 3$. The relation between the $V_{\rm Bg}$ range and a density change of 8e⁻/A is accurate to within 10% and allows us to determine $V_{\rm Bg}$ values corresponding to fractional fillings of the flat bands.

One of the surprising results of the experiment is the enhanced splitting between TDOS peaks around the CNP compared with the splitting of the fully occupied bands (Fig. 2d,e; see Supplementary Section 4 for details). This enhancement, marked by the relative shift of the TDOS peak positions as well as the increase of the overall width, stands out in a full bias-versus-back gate density map and hence has not been reported in transport measurements, which are only sensitive to energy scales of a few meV from the Fermi level. Exchange interactions are a plausible origin of the enhanced splitting at the CNP in analogy with quantum Hall ferromagnetism^{29,30}. In this scenario, the strong exchange interaction maximizes the separation between the bands when one of the flat bands is completely filled and the other completely empty. Two important differences distinguish TBG from quantum Hall systems. First, no external magnetic field is needed as flat bands are already present at zero

field; and second, the exchange interaction may not open a hard gap. Certain points in the Brillouin zone (away from the flat regions of the band causing the VHS) may remain gapless as a result of preserved symmetries^{25,31}.

We support this interpretation by calculations within the framework of a ten-band model for TBG developed in ref. 26 . While several effective models were proposed as starting points for studying TBG with and without interactions $^{27,32-35}$, the ten-band model 26 captures the non-interacting band structure of magic-angle TBG while going beyond the flat bands and incorporates all relevant symmetries. Although its overall bandwidth for the flat bands and the VHS peak splitting (7 meV and 1 mV, respectively) are small compared with our observations, the model provides qualitative guidance on interaction effects, including broken symmetries. To account for interaction effects, we have added a symmetry-preserving short-range interaction of strength $E_{\rm c}$ (see Supplementary Section 7 for details) and solved the model self-consistently within mean-field theory assuming that the symmetry between the four flavours (spin and valley) remains unbroken. We find several nearly degenerate

ARTICLES NATURE PHYSICS

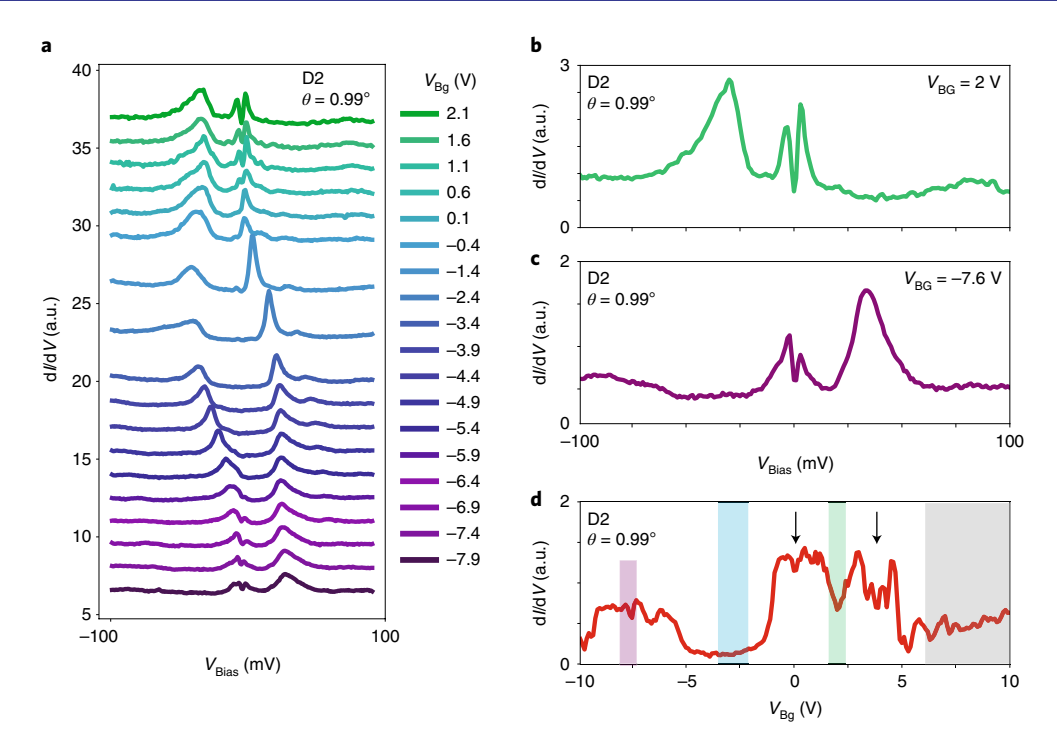


Fig. 4 | Spectroscopy at half-filling of the flat bands. a, Waterfall plot showing the evolution of point spectra as a function of V_{Bg} around the CNP for an AA site in an area with θ = 0.99° (device D2) and moiré unit cell lengths L_{MA} = 14.1 nm, L_{MB} = 14.1 nm and L_{MC} = 14.5 nm. **b,c**, Line cuts corresponding to half-filling on the electron and hole side. **d**, Conductance at the Fermi level (V_{Bias} = 0 mV) showing dips in the TDOS near half-filling on both the electron and hole side as indicated by the green and magenta rectangles (the blue and grey rectangles correspond to the CNP and full-filling). The black arrows indicate the expected positions corresponding to one-quarter and three-quarter filling.

broken-symmetry states (see Supplementary Section 7 for additional discussion). The solution breaking C_3 symmetry qualitatively reproduces the observed splitting near the CNP (Fig. 3). Other features such as the overall broadening of the bands near the CNP are also qualitatively captured. The resulting solution shows that the peaks in the local density of states (LDOS) are split by an amount set by E_c . For $1 < E_c/W < 2$, with W being the bandwidth of the non-interacting model, the relative increase in the splitting matches well with our experimental observations (Fig. 3a-c). The competitive energy of the C3-breaking solution suggests a high susceptibility towards nematicity^{36,37}; effects such as sample strain and unaccounted electronic correlations can plausibly stabilize this order as the unique ground state. Figure 3d,e shows the corresponding band structure across the Brillouin zone, with the Dirac cones protected by C_2T symmetry as indicated by the black dots. Moreover, the model predicts that the spatially varying breaking of the C_3 symmetry is most pronounced in the LDOS at the domain walls connecting different AA sites for energies close to VHS peaks, as calculated in Fig. 3f.

Consistent with these theoretical findings, spatially resolved TDOS maps taken on sites within the most C_3 -symmetric moiré regions show anisotropic TDOS profiles near the CNP (Fig. 3g). Experimentally, the most pronounced anisotropy is observed near the Fermi level when the TDOS at AA sites is suppressed, thus highlighting the domain wall areas. However, small energy-dependent variations for different directions are noticeable even when the TDOS at AA sites is larger, which indicates competition between the effects of strain and electronic correlations. The most pronounced domain-wall direction changes depending on whether $V_{\rm Bias}$ is adjusted to probe the lower or upper flat-band peak as expected from the model calculations (Fig. 3f). We note that the moiré periodicities in this particular area are $L_{\rm MA} = 13.8$ nm, $L_{\rm MB} = 13.7$ nm and $L_{\rm MC} = 14.2$ nm, indicating the presence of only 0.1–0.2% of uniaxial heterostrain 38,39 . These values of external strain correspond to

energy scales of 0.1–0.5 meV, which is much smaller than the energies corresponding to TBG lattice relaxation effects²⁸ or electronic correlations measured here. This implies that strain alone is unlikely to explain the measured anisotropies and suggests the formation of a nematic ground state of TBG near the CNP.

Finally, we focus on the states near half-filling of the flat bands (Fig. 4). Figure 4a shows the point spectroscopy as a function of $V_{\rm Bg}$ for a moiré site with a local twist angle θ =0.99° (device D2, $L_{\rm MA}$ =14.1 nm, $L_{\rm MB}$ =14.1 nm and $L_{\rm MC}$ =14.5 nm). In addition to the interaction-enhanced splitting at the CNP, a suppression in the TDOS is observed near half-filling both for electrons and holes, which signals the emergence of correlated gaps. Line cuts close to half-filling (Fig. 4b,c) show gap values between 4 and 8 meV that are higher than the values extracted from thermal activation in transport experiments 1.3. We suspect that this difference reflects effective disorder averaging over the sample area in transport measurements, which naturally reveals a reduced gap.

To better resolve the dependence on the filling of the flat band, we plot the zero-bias TDOS as a function of $V_{\rm Bg}$ in Fig. 4d. The trace shows local minima of the zero-bias TDOS for half-filling of the flat bands, consistent with correlated ground states at these fillings. The observed gaps typically occur near half-filling, although they are sometimes offset, presumably due to local electrostatic disorder, strain or tip-related effects. Occasionally, the less-developed states at one-quarter and three-quarter filling may also be resolved (black arrows in Fig. 4d). These observations strongly indicate that the measured gaps originate from correlated states at commensurate fillings and are distinct from other effects such as the Coulomb gap⁴⁰ that can also suppress the TDOS near the Fermi level in two-dimensional systems with strong electronic correlations^{41–46}.

Our results provide a local, spatially resolved picture of the electronic phases of TBG near the magic angle. We found that the band structure of the flat bands is considerably broader than anticipated

and comparable to the Coulomb interaction energy scale. At halffilling, we observed gaps for both electrons and holes that are consistent with the emergence of correlated insulating states as found in previous transport measurements. In addition, our results show that these interaction effects are robust against small deviations (of order 0.1°) from the magic angle. This suggests that strain and disorder play more important roles in observing the correlated states than an exact angle alignment. For twist angles below 0.9-1°, however, the bandgap between the dispersive and flat bands becomes considerably smaller²⁸. This sets a lower bound on the twist-angle range for which correlated flat-band physics can be accessed, as the additional bands become relevant for smaller angles^{5,28}. At charge neutrality, our results indicate that the ground state exhibits nematic order and breaks C₃ symmetry due to exchange interactions. These brokensymmetry states at the CNP have not yet been observed in transport measurements but may be visible via conductance anisotropy in very clean samples. Theoretically, one would expect that a similar exchange-driven mechanism opens a hard gap at fractional fillings when spin and valley degrees of freedom are taken into account^{29,47}. How superconductivity emerges from such symmetry-broken correlated insulating states remains an open question.

Note added in proof: During the preparation of this manuscript we become aware of a related work⁴⁸.

Online content

Any methods, additional references, Nature Research reporting summaries, source data, statements of code and data availability and associated accession codes are available at https://doi.org/10.1038/s41567-019-0606-5.

Received: 28 January 2019; Accepted: 26 June 2019; Published online: 5 August 2019

References

- Cao, Y. et al. Correlated insulator behaviour at half-filling in magic-angle graphene superlattices. *Nature* 556, 80–84 (2018).
- Cao, Y. et al. Unconventional superconductivity in magic-angle graphene superlattices. *Nature* 556, 43–50 (2018).
- Yankowitz, M. et al. Tuning superconductivity in twisted bilayer graphene. Science 363, 1059–1064 (2019).
- Trambly de Laissardière, G., Mayou, D. & Magaud, L. Localization of Dirac electrons in rotated graphene bilayers. *Nano Lett.* 10, 804–808 (2010).
- Bistritzer, R. & MacDonald, A. H. Moiré bands in twisted double-layer graphene. Proc. Natl Acad. Sci. USA 108, 12233–12237 (2011).
- Lopes dos Santos, J. M. B., Peres, N. M. R. & Castro Neto, A. H. Continuum model of the twisted graphene bilayer. *Phys. Rev. B* 86, 155449 (2012).
- Fang, S. & Kaxiras, E. Electronic structure theory of weakly interacting bilayers. *Phys. Rev. B* 93, 235153 (2016).
- 8. Neto, A. C., Guinea, F., Peres, N. M., Novoselov, K. S. & Geim, A. K. The electronic properties of graphene. *Rev. Mod. Phys.* 81, 109–162 (2009).
- Luican, A. et al. Single-layer behavior and its breakdown in twisted graphene layers. Phys. Rev. Lett. 106, 126802 (2011).
- 10. Li, G. et al. Observation of Van Hove singularities in twisted graphene layers. *Nat. Phys.* $\bf 6$, 109–113 (2010).
- Brihuega, I. et al. Unraveling the intrinsic and robust nature of van Hove singularities in twisted bilayer graphene by scanning tunneling microscopy and theoretical analysis. *Phys. Rev. Lett.* 109, 196802 (2012).
- Ohta, T. et al. Evidence for interlayer coupling and moiré periodic potentials in twisted bilayer graphene. *Phys. Rev. Lett.* 109, 186807 (2012).
- Havener, R. W., Liang, Y., Brown, L., Yang, L. & Park, J. Van Hove singularities and excitonic effects in the optical conductivity of twisted bilayer graphene. *Nano Lett.* 14, 3353–3357 (2014).
- Wong, D. et al. Local spectroscopy of moiré-induced electronic structure in gate-tunable twisted bilayer graphene. Phys. Rev. B 92, 155409 (2015).
- Kim, K. et al. Tunable moiré bands and strong correlations in small-twistangle bilayer graphene. Proc. Natl Acad. Sci. USA 114, 3364–3369 (2017).
- Huang, S. et al. Topologically protected helical states in minimally twisted bilayer graphene. Phys. Rev. Lett. 121, 037702 (2018).
- 17. Cao, Y. et al. Superlattice-induced insulating states and valley-protected orbits in twisted bilayer graphene. *Phys. Rev. Lett.* 117, 116804 (2016).
- Lopes dos Santos, J. M. B., Peres, N. M. R. & Castro Neto, A. H. Graphene bilayer with a twist: electronic structure. *Phys. Rev. Lett.* 99, 256802 (2007).

- Suárez Morell, E., Correa, J. D., Vargas, P., Pacheco, M. & Barticevic, Z. Flat bands in slightly twisted bilayer graphene: tight-binding calculations. *Phys. Rev. B* 82, 121407 (2010).
- Trambly de Laissardière, G., Mayou, D. & Magaud, L. Numerical studies of confined states in rotated bilayers of graphene. *Phys. Rev. B* 86, 125413 (2012).
- 21. Yan, W. et al. Angle-dependent van Hove singularities in a slightly twisted graphene bilayer. *Phys. Rev. Lett.* **109**, 126801 (2012).
- Yin, L.-J., Qiao, J.-B., Zuo, W.-J., Li, W.-T. & He, L. Experimental evidence for non-Abelian gauge potentials in twisted graphene bilayers. *Phys. Rev. B* 92, 081406 (2015)
- Zibrov, A. A. et al. Robust fractional quantum Hall states and continuous quantum phase transitions in a half-filled bilayer graphene Landau level. *Nature* 549, 360–364 (2017).
- Yoo, H. et al. Atomic and electronic reconstruction at the van der Waals interface in twisted bilayer graphene. Nat. Mater. 18, 448–453 (2019).
- Zou, L., Po, H. C., Vishwanath, A. & Senthil, T. Band structure of twisted bilayer graphene: emergent symmetries, commensurate approximants, and Wannier obstructions. *Phys. Rev. B* 98, 085435 (2018).
- Po, H. C., Zou, L., Senthil, T. & Vishwanath, A. Faithful tight-binding models and fragile topology of magic-angle bilayer graphene. *Phys. Rev. B* 99, 195455 (2019).
- Kang, J. & Vafek, O. Symmetry, maximally localized Wannier states, and a low-energy model for twisted bilayer graphene narrow bands. *Phys. Rev. X* 8, 031088 (2018).
- Nam, N. N. T. & Koshino, M. Lattice relaxation and energy band modulation in twisted bilayer graphene. *Phys. Rev. B* 96, 075311 (2017).
- Xie, M. & MacDonald, A. H. On the nature of the correlated insulator states in twisted bilayer graphene. Preprint at https://arxiv.org/abs/1812.04213 (2018).
- Song, Y. J. et al. High-resolution tunnelling spectroscopy of a graphene quartet. *Nature* 467, 185–189 (2010).
- Po, H. C., Zou, L., Vishwanath, A. & Senthil, T. Origin of Mott insulating behavior and superconductivity in twisted bilayer graphene. *Phys. Rev. X* 8, 031089 (2018).
- Kang, J. & Vafek, O. Strong coupling phases of partially filled twisted bilayer graphene narrow bands. *Phys. Rev. Lett.* 122, 246401 (2019).
- Koshino, M. et al. Maximally localized Wannier orbitals and the extended Hubbard model for twisted bilayer graphene. *Phys. Rev. X* 8, 031087 (2018).
- Guinea, F. & Walet, N. R. Electrostatic effects, band distortions, and superconductivity in twisted graphene bilayers. *Proc. Natl Acad. Sci. USA* 115, 13174–13179 (2018).
- Hejazi, K., Liu, C., Shapourian, H., Chen, X. & Balents, L. Multiple topological transitions in twisted bilayer graphene near the first magic angle. *Phys. Rev. B* 99, 035111 (2019).
- Lilly, M. P., Cooper, K. B., Eisenstein, J. P., Pfeiffer, L. N. & West, K. W. Anisotropic states of two-dimensional electron systems in high Landau levels: effect of an in-plane magnetic field. *Phys. Rev. Lett.* 83, 824–827 (1999).
- 37. Feldman, B. E. et al. Observation of a nematic quantum Hall liquid on the surface of bismuth. *Science* **354**, 316–321 (2016).
- Huder, L. et al. Electronic spectrum of twisted graphene layers under heterostrain. Phys. Rev. Lett. 120, 156405 (2018).
- Artaud, A. et al. Universal classification of twisted, strained and sheared graphene moiré superlattices. Sci. Rep. 6, 25670 (2016).
- Efros, A. L. Coulomb gap in disordered systems. J. Phys. C 9, 2021–2030 (1976).
- Ashoori, R. C., Lebens, J. A., Bigelow, N. P. & Silsbee, R. H. Equilibrium tunneling from the two-dimensional electron gas in GaAs: evidence for a magnetic-field-induced energy gap. *Phys. Rev. Lett.* 64, 681–684 (1990).
- Eisenstein, J. P., Pfeiffer, L. N. & West, K. W. Coulomb barrier to tunneling between parallel two-dimensional electron systems. *Phys. Rev. Lett.* 69, 3804–3807 (1992).
- Dial, O. E., Ashoori, R. C., Pfeiffer, L. N. & West, K. W. High-resolution spectroscopy of two-dimensional electron systems. *Nature* 448, 176–179
- 44. Song, Y.-H. et al. Observation of Coulomb gap in the quantum spin Hall candidate single-layer 1T'-WTe, Nat. Commun. 9, 4071 (2018).
- Moon, B. H. et al. Soft Coulomb gap and asymmetric scaling towards metal-insulator quantum criticality in multilayer MoS₂. Nat. Commun. 9, 2052 (2018).
- Jung, S. et al. Evolution of microscopic localization in graphene in a magnetic field from scattering resonances to quantum dots. *Nat. Phys.* 7, 245–251 (2011).
- Thomson, A., Chatterjee, S., Sachdev, S. & Scheurer, M. S. Triangular antiferromagnetism on the honeycomb lattice of twisted bilayer graphene. *Phys. Rev. B* 98, 075109 (2018).
- Kerelsky, A. et al. Magic angle spectroscopy. Preprint at https://arxiv.org/ abs/1812.08776 (2018).

ARTICLES NATURE PHYSICS

Acknowledgements

We gratefully acknowledge discussions with R. C. Ashoori, P. Jarillo-Herrero, A. Vishwanath, J. Eisenstein, A. Young and H. Beidenkopf. The STM work is in part supported by NSF DMR-1744011. Sample fabrication efforts are supported by the NSF through program NSF CAREER DMR-1753306. S.N.-P. acknowledges support from a KNI-Weathley fellowship. J.A., G.R., Fv.O., S.N.-P. and H.R. acknowledge the support of IQIM (NSF funded physics frontiers center). J.K. acknowledges support from the Deutsche Forschungsgemeinschaft (DFG 406557161), Y.C. a Kwanjeong fellowship, Fv.O. DFG support through CRC 183, and J.A. support from the Army Research Office under grant award W911NF-17-1-0323 and the NSF through grant DMR-1723367. Y.P., A.T. and J.A. are grateful for support from the Walter Burke Institute for Theoretical Physics at Caltech.

Author contributions

Y.C., J.K. and S.N.-P. conceived the experiment. Y.C. and J.K. performed the measurements. Y.C. made the samples with the help of H.A., R.P. and Y.Z. Y.C., J.K., H.R.

and S.N.-P. performed data analysis. Y.P. and A.T. developed the theory guided by F.v.O., J.A. and G.R. Y.C., J.K. and S.N.-P. wrote the manuscript with input from all authors.

Competing interests

The authors declare no competing interests.

Additional information

Supplementary information is available for this paper at https://doi.org/10.1038/s41567-019-0606-5.

Reprints and permissions information is available at www.nature.com/reprints.

Correspondence and requests for materials should be addressed to S.N.-P.

Publisher's note: Springer Nature remains neutral with regard to jurisdictional claims in published maps and institutional affiliations.

© The Author(s), under exclusive licence to Springer Nature Limited 2019

Methods

The samples were made using a tear-and-twist technique following similar procedures outlined in ref. ⁴⁹. The measurements were performed in a Unisoku USM 1300J STM/AFM system in STM mode. We used a Pt/Ir tip prepared on a Ag crystal by observing quasiparticle interference and a spectrum that shows the Ag(111) surface state. Before approaching the TBG sample, we verified that the DOS of the tip was featureless in the range of ± 200 mV by taking spectra of the gold electrodes before and after the measurements. We measured in total five devices and three of them showed a moiré pattern with a period close to 13 nm corresponding to a twist angle $\theta \approx 1.1^\circ$. Two of these devices were gate tunable in the range ± 10 V. The effective electron temperature of the system T=1.5 K was calibrated on the superconducting gap of a Pb(110) crystal mounted in a similar measurement configuration as the TBG. The lock-in parameters were: excitation voltage $V_{ac}=400\,\mu\text{V}-1\,\text{mV}$ and frequency $f=433\,\text{Hz}$. The scanner was calibrated on the atomic structure of the Pb(110) crystal. In all graphs, the twist angle θ is precise up to $\pm 0.02^\circ$.

Data availability

The experimental data and analyses that support the plots within this paper and the findings of this study are available from the corresponding author upon reasonable request.

Code availability

The computer codes that support the plots within this paper and the findings of this study are available from the corresponding author upon reasonable request

References

49. Kim, K. et al. Van der Waals heterostructures with high accuracy rotational alignment. *Nano Lett.* **16**, 1989–1995 (2016).